HHS Public Access

Author manuscript

FASEB J. Author manuscript; available in PMC 2023 August 15.

Published in final edited form as:

FASEB J. 2022 October ; 36(10): e22543. doi:10.1096/fj.202200841R.

Lipids uniquely alter secondary structure and toxicity of lysozyme aggregates

Mikhail Matveyenka[1], **Kiryl Zhaliazka**[1], **Stanislav Rizevsky**[1,2], **Dmitry Kurouski**[1,3]

[1]Department of Biochemistry and Biophysics, Texas A&M University, College Station, Texas, USA

[2]Department of Biotechnology, Binh Duong University, Thu Dau Mot, Vietnam

[3]Department of Biomedical Engineering, Texas A&M University, College Station, Texas, USA

Abstract

Abrupt aggregation of misfolded proteins is a hallmark of the large group of amyloid pathologies that include diabetes type 2, Alzheimer and Parkinson's diseases. Protein aggregation yields oligomers and fibrils, β-sheet-rich structures that exert cell toxicity. Microscopic examination of amyloid deposits reveals the presence of lipids membranes, which suggests that lipids can be involved in the process of pathogenic protein assembly. In this study, we show that lipids can uniquely alter the aggregation rates of lysozyme, a protein that is associated with systemic amyloidosis. Specifically, cardiolipin (CL), ceramide (CER), and sphingomyelin (SM) accelerate, phosphatidylcholine (PC) strongly inhibits, whereas phosphatidylserine (PS) has no effect on the rate of protein aggregation. Furthermore, lipids uniquely alter the secondary structure of lysozyme aggregates. Furthermore, we found that lysozyme aggregates grown in the presence of CL, CER, SM, PS, and CL:PC mixtures exert significantly lower production of reactive oxygen species and mitochondrial dysfunction compared to lysozyme:PC aggregates and lysozyme fibrils grown in the lipid-free environment. These findings suggest that a change in the lipid composition of cell membranes, which is taken place upon neurodegeneration, may trigger the formation of toxic protein species that otherwise would not be formed.

Keywords

AFM-IR; amyloid aggregates; lipids; lysozyme; ROS; toxicity

Correspondence Dmitry Kurouski, Department of Biochemistry and Biophysics, Texas A&M University, College Station, TX 77843, USA. dkurouski@tamu.edu.

AUTHOR CONTRIBUTIONS

Mikhail Matveyenka designed the project and performed toxicity experiments, and analyzed data; Kiryl Zhaliazka performed kinetics, CD and FTIR experiments and analyzed data; Stanislav Rizevsky performed AFM and AFM-IR experiments and analyzed data; Dmitry Kurouski designed the project and analyzed data. All authors wrote the manuscript.

DISCLOSURES

The authors declare no competing financial interests.

SUPPORTING INFORMATION

Additional supporting information can be found online in the Supporting Information section at the end of this article.

1 | INTRODUCTION

Self-assembly of misfolded proteins into oligomers and fibrils is the molecular signature of a large group of pathologies that include type 2 diabetes, Alzheimer, Parkinson, and Huntington's diseases.[1-3] Over the past decade, excessive knowledge has been accumulated about the kinetic and thermodynamic nature of such protein assembly.[4,5] Specifically, the shape of the aggregation kinetics suggested that an assembly of amyloidogenic proteins starts from oligomers that, once reached a critical concentration in solution, rapidly propagate into filaments.[4,6-11] Cryo-electron microscopy and solid-state nuclear magnetic resonance (ss-NMR) allowed for the elucidation of the secondary structure of filaments with Angstrom spatial resolution.[12-14] It has been found that filaments have a cross-β-sheet secondary structure; they also can coil and intertwine minimizing their free energy, which results in the appearance of proto-fibrils and fibrils.[10,15]

A growing body of evidence suggests that lipids can alter rates of protein aggregation. Specifically, Galvagnion and co-workers found that lipids can either accelerate or decelerate the rate of α-synuclein (α-Syn) aggregation, the protein that is directly linked to Parkinson's disease (PD). In this case, the effect on the rate of protein aggregation is determined by the chemical structure of the lipid and a lipid-to-protein ratio.[16-18] Our group found that lipids not only alter the rates of α-Syn aggregation but also uniquely modify the secondary structure of protein oligomers.[5] Furthermore, oligomers that are formed in the presence of lipids possess lipids in their structure.[5]

A critical question is whether the lipid-mediated effect on the structure and aggregation kinetics is unique to α-Syn or whether it is a general phenomenon applicable to a large group of amyloid-associated proteins. To answer this question, we examined the effect of lipids on the aggregation rates of hen egg-white lysozyme, a small protein that has a 14.3 kDa molecular weight. Under low pH and elevated temperatures, lysozyme can be easily denatured which triggers its aggregation into oligomers and fibrils.[19,20] Using deep UV resonance Raman (DUVRR) spectroscopy, Xu and co-workers showed that this process is primarily triggered by the denaturation of α-helical domains and the assembly of unfolded protein sequences into cross-β-sheet.[21,22] 2D correlation DUVRR used by Shashilov and Lednev reveals that assembling, lysozyme first formed nuclei that templated protein assembly into fibrils.[23,24] It has been shown that pH can be used to alter the structure and supramolecular chirality of lysozyme fibrils.[20] Specifically, at pH below 2, lysozyme forms tape-like fibrils, whereas at pH above this point, protein aggregation yields left-twisted fibrils with the distinctly different supramolecular organization.

Under physiological conditions, lysozyme is exposed to cell and mitochondrial membranes that have high concentrations of phospholipids, such as cardiolipin (CL), phosphatidylcholine (PC), and phosphatidylserine (PS), as well as ceramide (CER), and sphingomyelin (SM).[25] Cardiolipin (CL) is a unique phospholipid that constitutes ~20% of the inner mitochondrial membrane.[26] It carries two negative charges playing an important role in cell respiration and energy conversion. Zwitterionic PC constitutes around 30% of the plasma and organelle membranes, whereas ~10% of the plasma membrane is occupied by PS.[27-29] Under physiological conditions, negatively charged PS is primarily localized on the

inner part of the membrane.[28,30,31] Its exposure to the exterior part of the plasma membrane indicates cell malfunction.[32] In such cases, PS is recognized by phagocytes that degrade such apoptotic and necrotic cells.[25] CER and SM occupy around 6% and 4% of the plasma membrane, respectively. These lipids form the myelin sheath that surrounds nerve cell axons where they perform an important role in signal transduction.[27-29]

Therefore, in our study, we tested the effect of these lipids, as well as their mixtures on lysozyme aggregation. We also used a set of spectroscopic, microscopic, and molecular methods to examine changes in the secondary structure, morphology, and toxicity of lysozyme aggregates grown in the presence of PC, PS, CL, as CER, and SM, as well as in the equimolar (1:1) and 1:4 molar mixtures of CL and PC. Our findings show that lipids drastically alter the aggregation rates, secondary structure, and morphology of lysozyme aggregates. These structurally different aggregates exert much lower cell toxicities than lysozyme fibrils grown in the lipid-free environment.

2 | EXPERIMENTAL SECTION

2.1 | Materials

Hen egg-white lysozyme was purchased from Sigma-Aldrich (St. Louis, MO, USA), 1,2-ditetradecanoyl-sn-glyc ero-3-phospho-L-serine (DMPS or PS), 1,2-Dimyristoyl-sn-glycero-3-phosphocholine (DMPC or PC), 1′,3′-bis[1,2-d istearoyl-sn-glycero-3-phospho]-glycerol (18:0 cardiolipin (CL)), sphingomyelin (SM), and ceramide (CER) were purchased from Avanti (Alabaster, AL, USA).

2.2 | Liposome preparation

DMPS, DMPC, and CL large unilamellar vesicles (LUVs) were prepared accordingly to the method reported by Galvagnion et al.[33] Briefly, 0.6 mg of the lipid were dissolved in 2.6 ml of phosphate-buffered saline (PBS) pH 7.4. Lipid solutions were heated in a water bath to ~50°C for 30 min and then placed into liquid nitrogen for 3–5 min. This procedure was repeated 10 times. After this, lipid solutions were passed 15 times through a 100 nm membrane that was placed into the extruder (Avanti, Alabaster, AL, USA). LUV sizes were determined by dynamic light scattering. Due to the poor assembly properties, no LUVs for SM and CER were prepared; lipids were used as received.

2.3 | Hen egg-white lysozyme aggregation

In the lipid-free environment, 400 μM of hen egg-white lysozyme was dissolved in PBS; the solution pH was adjusted to pH 3.0 using concentrated HCl. For Lys:CL, Lys:CER, Lys:PS, and Lys:SM, as well as for Lys:PC:CL (1:0.5:0.5) and Lys:PC:CL (1:0.8:0.2), 400 μM of lysozyme was mixed with an equivalent concentration of the corresponding lipid; solution pH was adjusted to pH 3.0 using concentrated HCl. Next, the solutions were placed in the dry block heater and kept at 65°C for 24 h.

2.4 | Kinetic measurements

Lysozyme aggregation was monitored using a thioflavin T (ThT) fluorescence assay. Prior to measurements, protein samples were mixed with 2 mM of ThT solution and placed in the

plate reader (Tecan, Männedorf, Switzerland). Fluorescence emission was collected at 488 nm with 450 nm excitation. All measurements were made in triplicates.

2.5 | Atomic force microscopy imaging

Atomic force microscopy (AFM) imaging was performed using silicon AFM probes with related parameters force constant 2.7 N/m and resonance frequency 50–80 kHz were purchased from Appnano (Mountain View, CA, USA) on the AIST-NT-HORIBA system (Edison, NJ). For each measurement, an aliquot of the sample after 24 h of incubation at 65°C was diluted with 1× PBS, pH 3.0, and deposited on the pre-cleaned silicon wafer. Next, the sample was dried under a flow of dry nitrogen. Analysis of collected images was performed using AIST-NT software (Edison, NJ, USA).

2.6 | Attenuated total reflectance Fourier-transform infrared spectroscopy

After 24 h of sample incubation, samples were placed onto ATR crystal and dried at room temperature. Spectra were measured using Spectrum 100 FTIR spectrometer (Perkin-Elmer, Waltham, MA, USA). Three spectra were collected from each sample.

2.7 | Atomic force microscopy infrared

Atomic force microscopy infrared (AFM-IR) imaging was conducted using a Nano-IR 3 system (Bruker, Santa Barbara, CA, USA). The IR source was a QCL laser. Contact-mode AFM tips (ContGB-G AFM probe, NanoAndMore, Watsonville, CA, USA) were used to obtain all spectra and maps. For each measurement, an aliquot of the sample after 24 h of incubation at 65°C was diluted with 1× PBS, pH 3.0, and deposited on the pre-cleaned silicon wafer. Next, the sample was dried under a flow of dry nitrogen. Treatment and analysis of the collected spectra were performed in Matlab (The Mathworks, Inc. Natick, Massachusetts, USA).

2.8 | Circular dichroism

After 24 h of sample incubation, samples were diluted to the final concentration of 100 μM using PBS and measured immediately using a J-1000 circular dichroism (CD) spectrometer (Jasco, Easton, MD, USA). Three spectra were collected for each sample within 205–250 nm.

2.9 | Cell toxicity assays

Mice midbrain N27 cells were grown in RPMI 1640 Medium (Thermo Fisher Scientific, Waltham, MA, USA) with 10% fetal bovine serum (FBS) (Invitrogen, Waltham, MA, USA) in 96 well-plate (5000 cells per well) at 37°C under 5% CO_2. After 24 h, the cells were found to fully adhere to the wells reaching ~70% confluency. Next, 100 μl of the cell culture was replaced with 100 μl RPMI 1640 Medium with 5% FBS containing protein samples. After 48 h of incubation, reactive oxygen species (ROS) assay was performed. Briefly, ROS reagent (C10422, Invitrogen, Waltham, MA, USA) was added to reach the final concentration of 5 μM and incubated at 37°C under 5% CO_2 for 30 min. After the supernatant was removed, cells were washed with PBS and resuspended in 200 μl of PBS in the flow cytometry tubes. Sample measurements were made in LSR II Flow Cytomter

(BD, San Jose, CA, USA) using a red channel (λ = 633 nm). Every well was measured 25 times in different locations. At least two independently prepared protein samples were examined using LDH assay. All measurements were made in triplicates. A T-test was used to determine the significance level of differences between the toxicity of analyzed samples. Percentages of ROS cells were determined using LSR II software. For JC-1 staining, 1 μl of JC-1 reagent (M34152A, Invitrogen, Waltham, MA, USA) was added to cells and incubated at 37°C under 5% CO_2 for 30 min. After the supernatant was removed, cells were washed with PBS and resuspended in 200 μl of PBS in the flow cytometry tubes. Sample measurements were made in LSR II Flow Cytomter (BD, San Jose, CA, USA) using a red channel (λ = 633 nm). JC-1 intensity was determined using LSR II software. All measurements were made in triplicates.

3 | RESULTS

3.1 | Kinetics of lysozyme aggregation

We first investigated whether lipids may alter the lag phase and rate of lysozyme aggregation. For this, lysozyme was mixed in 1:1 molar ratios with PC, PS, CL, SM, and CER, as well as with a mixture of PC:CL at 50:50 and 80:20 molar ratios. The solutions were then kept at 65°C under 510 rpm agitation. We found that lysozyme aggregation in the lipid-free environment had a prolonged lag phase that was followed by a rapid increase in the ThT intensity, which indicated a formation of protein aggregates, Figure 1A. We found that CL, SM, CER, and a mixture of PC:CL at 50:50 and 80:20 molar ratios significantly shortened the lag phase (t_{lag}) of lysozyme aggregation, Figure 1B. Specifically, the lag phase shortened from 11.7 ± 0.3 h (Lys) to 4.3 ± 0.1 h in the presence of SM and 3.9 ± 0.5 and 3.8 ± 0.3 h in the presence of CL and CER, respectively, Table S1. Lysozyme aggregation in the mixture of PC:CL at 50:50 and 80:20 molar ratios reached t_{lag} at 2.9 ± 0.3 h and 2.8 ± 0.5 h, respectively. Importantly, we found that PC completely inhibits lysozyme aggregation, whereas PS did not significantly alter t_{lag} of protein aggregation. These findings show that lipids can uniquely shorten and delay the lag phase of lysozyme aggregation or have no effect on t_{lag} of the protein assembly into fibrils. Similar results were recently reported by Matveyenka and co-workers for insulin.[34,35] Specifically, it was found that PC strongly inhibited insulin aggregation, whereas both CL and PS strongly accelerated insulin fibril formation.

We also observed that lipids alter rates of lysozyme aggregation. We found that CL ($t_{1/2}$ = 5.0 ± 0.5 h), CER ($t_{1/2}$ = 5.2 ± 0.2 h), SM ($t_{1/2}$ = 5.3 ± 0.3 h), PC:CL (50:50) ($t_{1/2}$ = 4.8 ± 0.5 h) and PC:CL (80:20) ($t_{1/2}$ = 4.7 ± 0.3 h) substantially accelerated the rate of lysozyme aggregation (Lysozyme $t_{1/2}$ = 13.7 ± 0.6 h), Figure 1B and Table S1. However, PS ($t_1/_2$ = 13.9 ± 0.5 h), did not exert significant changes on the rate of fibril formation, Table S1. These findings show that in addition to the effect on t_{lag}, lipids also uniquely alter the rate of lysozyme aggregation.

It should be noted that our ThT fluorescence measurements showed that intensities of products of lysozyme aggregation that took place in the presence of lipids are higher than the intensity of aggregates formed in the lipid-free environment. This finding suggests that lysozyme aggregation in the presence of lipids yields a higher amount of ThT active

protein aggregates. Similar results were recently reported by Matveyenka and co-workers for insulin.[34,35] Specifically, it was found that such an increase in the ThT intensity is associated with drastic changes in the morphology and secondary structure of inulin aggregates that were grown in the presence of PS and CL compared to the insulin fibrils formed in the lipid-free environment.

3.2 | Morphological analysis of lysozyme aggregates

AFM analysis of lysozyme aggregates grown in the presence of PS, CL, CER, and SM, as well as in the presence of lipid mixtures PC:CL at 1:1 and 0.8:0.2 revealed predominance of thick (20–40 nm in height) fibrils, Figure 2. We also found that some of these fibrils are self-assembled into thicker bundles. Lysozyme aggregates grown in the lipid-free environment showed a similar morphological appearance; the sample was dominated by 20–40 nm thick fibrils. At the same time, only oligomers (5–7 nm in height) were observed in the solution of lysozyme aggregated in the presence of PC. This observation shows that PC inhibits lysozyme fibril formation yielding the formation of only small oligomeric species. At the same time, these oligomers were able to accelerate lysozyme aggregation if used as seeds in a 1%–10% mol/mol ratio (Figures S1).

3.3 | Structural characterization of protein aggregates

We utilized CD and attenuated total reflectance Fourier-transform Infrared infrared (ATR-FTIR) to examine the secondary structure of lysozyme aggregates grown in the presence of lipids, as well as in a lipid-free environment. CD spectra collected from Lys, Lys:CER, Lys:PS, Lys:CL, Lys:PC:CL (1:0.5:0.5), and Lys:PC:CL (1:0.8:0.2) exhibited a trough at ~223 nm and a peak at ~205 nm, Figure 3A. These spectroscopic features demonstrate the dominance of β-sheet in the secondary structure of these aggregates.[36,37] However, Lys:SM and Lys:PC had the trough shifted to ~215 nm with a substantially lower intensity of 205 nm peak (Lys:SM) or the absence of this peak (Lys:PC). These spectroscopic signatures are characteristic of proteins with a mixture of α-helix, β-sheet, and unordered secondary structures.[36,37] Thus, we can conclude that Lys, Lys:CER, Lys:PS, Lys:CL, Lys:PC:CL (1:0.5:0.5) and Lys:PC:CL (1:0.8:0.2) are primarily composed of β-sheet. At the same time, Lys:SM and especially Lys:PC possess a substantial amount of α-helix and unordered secondary structures in addition to the β-sheet.

ATR-FTIR analysis of lysozyme aggregates grown in the presence of lipids, as well as in the lipid-free environment confirmed the discussed above CD results, Figure 3B. In the ATR-FTIR spectrum collected from Lys:PC, we observed the amide I band centered ~1657 cm^{-1} with a shoulder at ~1625 cm^{-1}. This indicates the predominance of α-helix and unordered secondary structures with a small content of β-sheet in Lys:PC.[38,39] In the spectra collected from Lys, Lys:PS, Lys:CER, Lys:SM, Lys:CL, as well as Lys:PC:CL (1:0.5:0.5) and Lys:PC:CL (1:0.8:0.2) amide I was centered at ~1625 cm^{-1}, which indicates the dominance of parallel β-sheet secondary structure in these protein aggregates.[38,40] Finally, we found that lysozyme aggregates grown in the absence of lipids demonstrated spectra with drastically different amide II bands. Specifically, we found that intensities of 1550 and 1525 cm^{-1} bands were nearly identical in the spectrum collected from Lys, whereas the intensity of 1550 cm^{-1} was found to be larger than the 1525 cm^{-1} band in the spectra collected

from all lysozyme aggregates that were grown in the presence of lipids. This makes us conclude that lysozyme aggregates grown in the lipid-free environment are structurally different from Lys:PS, Lys:CER, Lys:SM, Lys:CL, as well as Lys:PC:CL (1:0.5:0.5) and Lys:PC:CL (1:0.8:0.2). Finally, Lys:PC structures are drastically different from the structures of lysozyme aggregates grown in the presence of other lipids, which is in a good agreement with our AFM results.

The question to ask is whether lipids present in the structure of the lysozyme aggregates that were grown in the presence of lipids. To answer this question, we used atomic force microscopy Infrared (AFM-IR) spectroscopy.[41-43] AFM-IR allows for positioning the metalized scanning probe directly on the sample of interest.[44,45] Next, the sample is illuminated by pulsed tunable IR light that causes thermal expansions in the protein aggregate which, in turn, are recorded by the scanning probe. The thermal expansions can be converted to the IR spectrum of the aggregate which allows for probing its structure and composition.[5,42,46,47]

AFM-IR spectra collected from individual lysozyme aggregates that were grown in the presence of lipids exhibited vibrational bands centered ~800 and 1000–1200 cm^{-1}, Figure 4. These vibrational bands correspond to C-H and PO_2^- vibration respectively.[46,48] We have found that Lys:PS, Lys:CER, and Lys:SM exhibited very strong intensities of ~800 and 1000–1200 cm^{-1} bands. This finding point to the presence of a significant amount of the corresponding lipids in the structure of these aggregates. We also found that intensities of 1000–1200 cm^{-1} bands were substantially lower in the spectra collected from Lys:PC, Lys:CL, Lys:PC:CL (1:0.5:0.5), and Lys:PC:CL (1:0.8:0.2) comparing to the intensities of these bands in the spectra collected from Lys:PS, Lys:CER, and Lys:SM. These findings show that CL and PC do not accumulate in the structure of lysozyme aggregates that are grown in the presence of these lipids. Thus, lysozyme fibrils are grown in the presence of CL and PC, as well as PC:CL (1:1) and PC:CL (0.8:0.2) have very little if any lipid in their structure.

In addition to the compositional analysis, AFM-IR allows for the elucidation of the structural heterogeneity of the analyzed protein aggregates. The structural heterogeneity can be determined by variability in the intensity in observed vibrational bands that correspond to lipids (~800 and 1000–1200 cm^{-1}) and protein (1555 cm^{-1} (amide II) and 1630–1595 cm^{-1} (amide I)) vibrations.[34,35,48,49] We found that lysozyme aggregates grown in the lipid-free environment exhibited very little if any structural heterogeneity. However, structural heterogeneity of Lys:PS, Lys:CL, as well as Lys:PC:CL (1:0.5:0.5) and Lys:PC:CL (1:0.8:0.2) was found to be substantially larger. Finally, we found that lysozyme aggregates that were grown in the presence of SM and especially CER exhibited the largest structural variability among all analyzed classes of lysozyme aggregates.

3.4 | Toxicity of lysozyme aggregates

We utilize a mice midbrain N27 cell line and a set of toxicity assays to examine the relationship between the structure and toxicity of lysozyme aggregates. Amyloid aggregates exert toxicities by enhancing ROS production and inducing mitochondrial dysfunction in

cells.[4,34,35,50] Therefore, we examined the extent to which these structures are engaged in ROS production and mitochondrial dysfunction of cells, Figure 5.

ROS test indicated that Lys:CL, Lys:PC:CL (1:0.5:0.5), and Lys:SM and Lys:CER exhibited significantly lower levels of ROS production compared to lysozyme aggregates grown in the lipid-free environment (Lys), Figure 5. We also found that ROS production by Lys:CL:PC (1:0.2:0.8), Lys:PC, and Lys:PS was not significantly different from the ROS levels associated with Lys themselves. These results show that some lipids, specifically CL, CER, and SM are capable of reducing ROS associated with amyloid aggregates in cells, whereas other lipids such as PC and PS do not exhibit such properties. This conclusion can be also made about lysozyme aggregates grown in the presence of lipid mixtures. Specifically, a high relative concentration of CL relative to PC in the lipid mixture (Lys:PC:CL (1:0.5:0.5)) allows for stronger suppression of ROS production compared to the one observed for Lys:CL:PC (1:0.2:0.8) where CL is 4 times lower than the concentration of PC. It should be noted that most lipids themselves did not exert any cell toxicity, except CL and PC which exhibited significant cell toxicity relative to the control (butter).

We also utilized JC-1 dye to examine the mitochondrial dysfunction caused by lysozyme aggregates. It was found that lysozyme aggregates grown in the lipid-free environment exert significantly higher mitochondrial dysfunction compared to the protein aggregates grown in the absence of CL, CL:PC (1:0.5:0.5), CL:PC (1:0.2:0.8), PS, SM, and CER. It should be noted that only Lys:PC did not exert significantly lower cell toxicity compared to the lysozyme aggregates grown in the lipid-free environment. Thus, all tested lipids and lipid mixtures except PC can mitigate mitochondrial dysfunction caused by amyloid aggregates. Our JC-1 results also show that all tested lipids themselves cause significant mitochondrial dysfunction which is yet much lower compared to the stresses caused by their mixtures with lysozyme and lysozyme aggregates themselves.

4 | DISCUSSION

Our experimental results show that rates of protein aggregation, as well as the secondary structure and toxicity of lysozyme aggregates, can be uniquely altered by lipids if the protein aggregates in their presence. Specifically, we found that most lipids, such as CL, SM, CER, as well as lipid mixtures (Lys:CL:PC (1:0.5:0.5), Lys:CL:PC (1:0.2:0.8)), accelerate the rates of lysozyme aggregation. Other lipids, such as PS, exert no effect on the rate of lysozyme aggregation, whereas PC strongly inhibits protein aggregation. These effects are reflected in the secondary structure of the corresponding aggregates. Specifically, Lys:PC has a mixture of β-sheet, α-helix, and unordered protein secondary structure, whereas the structures of Lys, Lys:CL, Lys:PS, Lys:SM, Lys:CER, Lys:CL:PC (1:0.5:0.5), and Lys:CL:PC (1:0.2:0.8) are dominated by parallel β-sheet secondary structure. It should be noted that the secondary structure of lysozyme aggregates grown in the lipid-free environment is different from the secondary structure of the discussed above protein aggregates that were formed in the presence of lipids. AFM-IR aggregates show that this difference can arise from the presence of lipids in the structure of lysozyme aggregates that were grown in their presence.

These findings are significant because aggregation of a large number of amyloidogenic proteins and peptides, such as α-synuclein and amyloid β, is taken place at the interfaces between lipid membranes and aqueous media. There is also a growing body of evidence that the lipid profile of membranes changes with aging. Thus, one can expect that the presence of some lipids, such as SM and CER in lipid membranes, helps mitigate the toxicities of proteins that aggregate in their presence. At the same time, the effect of other lipids, such as PC, is not evident in regards to toxicities of the formed protein aggregates. Nevertheless, PC causes drastic changes in the secondary structure and morphology of lysozyme aggregates formed in the presence of this lipid.

In summary, our results show that lipids exert three major effects on lysozyme aggregation. First, lipids uniquely accelerate or decelerate protein aggregation. This effect directly depends on the lipid structure. Second, lipids alter the secondary structure of lysozyme aggregates, and third, toxicities that these aggregates exert in cells. In these cases, the degree of toxicity does not have a direct relationship with the secondary structure of the aggregates or the rate of their formation. This evidence suggests that the toxicity of the lipid-protein aggregates is determined by the structure of the lipids present in their structure. Such interactions are developed between charged amino acid residues of proteins and polar head groups of lipids. For instance, lysine and glutamic acid residues on the N-terminus (amino acids 1–60) of α-Syn exhibit strong electrostatic interactions with headgroups of phospholipids that triggers α-Syn aggregation.[51] NMR and fluorescence methods also revealed that lipid-protein interactions are facilitated by hydrophobic interactions between non-polar amino acid residues of the protein and fatty acid tails of lipids.[52,53]

An uptake of amyloid aggregates by cells typically occurs by their endocytosis. Our findings suggest that lysozyme aggregates damage endosomes which make the aggregates leak in into the cytosol where they induce ROS production and cause mitochondrial damage, Figure 6.

5 | CONCLUSIONS

Our experimental findings show that lipids uniquely alter both the lag phase and rate of lysozyme aggregation. We also found that in the presence of lipids, lysozyme forms structurally and morphologically different aggregates that have significantly lower cell toxicities than fibrils grown in the lipid-free environment. We also found that the level of ROS production and mitochondrial damage is dictated by the lipid-protein complex that is different for different lipids. These findings suggest that irreversible changes in lipid profiles of organs may trigger the formation of toxic protein species that in turn are responsible for the onset and progression of amyloidogenic diseases.

Supplementary Material

Refer to Web version on PubMed Central for supplementary material.

ACKNOWLEDGMENT

We are grateful to the National Institute of Health for the provided financial support (R35GM142869).

DATA AVAILABILITY STATEMENT

All data in this study can be provided by the corresponding author if needed.

Abbreviations:

AFM	atomic force microscopy
AFM-IR	atomic force microscopy Infrared spectroscopy
ATR-FTIR	attenuated total reflectance Fourier-transform infrared spectroscopy
CD,	circular dichroism
CER	ceramide
CL	cardiolipin
LUVs	large unilamellar vesicles
Lys	lysozyme
PC	phosphatidylcholine
PS	phosphatidylserine
ROS	reactive oxygen species
SM	sphingomyelin
t1/2	time when the intensity of ThT fluorescence reached 50% of the maximum
tgrow	time when the intensity of ThT fluorescence reached 90% of the maximum
ThT	thioflavin T
tlag	time when the intensity of ThT fluorescence reached 10% of the maximum

REFERENCES

1. Chiti F, Dobson CM. Protein misfolding, amyloid formation, and human disease: a summary of progress over the last decade. Annu Rev Biochem. 2017;86:27–68. [PubMed: 28498720]
2. Knowles TP, Vendruscolo M, Dobson CM. The amyloid state and its association with protein misfolding diseases. Nat Rev. 2014;15:384–396.
3. Iadanza MG, Jackson MP, Hewitt EW, Ranson NA, Radford SE. A new era for understanding amyloid structures and disease. Nat Rev Mol Cell Biol. 2018;19:755–773. [PubMed: 30237470]
4. Chen SW, Drakulic S, Deas E, et al. Structural characterization of toxic oligomers that are kinetically trapped during alpha-synuclein fibril formation. Proc Natl Acad Sci U S A. 2015;112:E1994–E2003. [PubMed: 25855634]

5. Dou T, Zhou L, Kurouski D. Unravelling the structural organization of individual alpha-synuclein oligomers grown in the presence of phospholipids. J Phys Chem Lett. 2021;12:4407–4414. [PubMed: 33945282]
6. Pieri L, Madiona K, Melki R. Structural and functional properties of prefibrillar α-synuclein oligomers. Sci Rep. 2016;6:24526. [PubMed: 27075649]
7. Cremades N, Cohen SI, Deas E, et al. Direct observation of the interconversion of normal and toxic forms of alpha-synuclein. Cell. 2012;149:1048–1059. [PubMed: 22632969]
8. Apetri MM, Maiti NC, Zagorski MG, Carey PR, Anderson VE. Secondary structure of alpha-synuclein oligomers: characterization by raman and atomic force microscopy. J Mol Biol. 2006;355:63–71. [PubMed: 16303137]
9. O'Leary EI, Lee JC. Interplay between alpha-synuclein amyloid formation and membrane structure. Biochim Biophys Acta Prot Proteom. 2019;1867:483–491.
10. Kurouski D, Van Duyne RP, Lednev IK. Exploring the structure and formation mechanism of amyloid fibrils by Raman spectroscopy: a review. Analyst. 2015;140:4967–4980. [PubMed: 26042229]
11. Hong DP, Han S, Fink AL, Uversky VN. Characterization of the non-fibrillar alpha-synuclein oligomers. Prot Pept Lett. 2011;18:230–240.
12. Li B, Ge P, Murray KA, et al. Cryo-EM of full-length alpha-synuclein reveals fibril polymorphs with a common structural kernel. Nat Commun. 2018;9:3609. [PubMed: 30190461]
13. Guerrero-Ferreira R, Taylor NM, Mona D, et al. Cryo-EM structure of alpha-synuclein fibrils. Elife. 2018;7:e36402. [PubMed: 29969391]
14. Tycko R. Solid-state NMR studies of amyloid fibril structure. Annu Rev Phys Chem. 2011;62:279–299. [PubMed: 21219138]
15. Paravastu AK, Qahwash I, Leapman RD, Meredith SC, Tycko R. Seeded growth of beta-amyloid fibrils from Alzheimer's brain-derived fibrils produces a distinct fibril structure. Proc Natl Acad Sci U S A. 2009;106:7443–7448. [PubMed: 19376973]
16. Alza NP, Iglesias Gonzalez PA, Conde MA, Uranga RM, Salvador GA. Lipids at the crossroad of alpha-synuclein function and dysfunction: biological and pathological implications. Front Cell Neurosci. 2019;13:175. [PubMed: 31118888]
17. Galvagnion C. The role of lipids interacting with alpha-synuclein in the pathogenesis of Parkinson's disease. J Parkinsons Dis. 2017;7:433–450. [PubMed: 28671142]
18. Galvagnion C, Brown JW, Ouberai MM, et al. Chemical properties of lipids strongly affect the kinetics of the membrane-induced aggregation of alpha-synuclein. Proc Natl Acad Sci U S A. 2016;113:7065–7070. [PubMed: 27298346]
19. Mulaj M, Foley J, Muschol M. Amyloid oligomers and protofibrils, but not filaments, self-replicate from native lysozyme. J Am Chem Soc. 2014;136:8947–8956. [PubMed: 24884889]
20. Kurouski D, Lu X, Popova L, et al. Is supramolecular filament chirality the underlying cause of major morphology differences in amyloid fibrils? J Am Chem Soc. 2014;136:2302–2312. [PubMed: 24484302]
21. Xu M, Shashilov V, Lednev IK. Probing the cross-beta core structure of amyloid fibrils by hydrogen-deuterium exchange deep ultraviolet resonance Raman spectroscopy. J Am Chem Soc. 2007;129:11002–11003. [PubMed: 17705492]
22. Xu M, Shashilov VA, Ermolenkov VV, Fredriksen L, Zagorevski D, Lednev IK. The first step of hen egg white lysozyme fibrillation, irreversible partial unfolding, is a two-state transition. Protein Sci. 2007;16:815–832. [PubMed: 17400924]
23. Shashilov V, Xu M, Ermolenkov VV, Fredriksen L, Lednev IK. Probing a fibrillation nucleus directly by deep ultraviolet Raman spectroscopy. J Am Chem Soc. 2007;129:6972–6973. [PubMed: 17500518]
24. Shashilov VA, Lednev IK. 2D correlation deep UV resonance raman spectroscopy of early events of lysozyme fibrillation: kinetic mechanism and potential interpretation pitfalls. J Am Chem Soc. 2008;130:309–317. [PubMed: 18067295]
25. Fitzner D, Bader JM, Penkert H, et al. Cell-type- and brain-region-resolved mouse brain lipidome. Cell Rep. 2020;32:108132. [PubMed: 32937123]

26. Pope S, Land JM, Heales SJ. Oxidative stress and mitochondrial dysfunction in neurodegeneration; cardiolipin a critical target? Biochim Biophys Acta. 2008;1777:794–799. [PubMed: 18420023]
27. La Rosa C, Scalisi S, Lolicato F, Pannuzzo M, Raudino A. Lipid-assisted protein transport: A diffusion-reaction model supported by kinetic experiments and molecular dynamics simulations. J Chem Phys. 2016;144:184901. [PubMed: 27179503]
28. Michaelson DM, Barkai G, Barenholz Y. Asymmetry of lipid organization in cholinergic synaptic vesicle membranes. Biochem J. 1983;211:155–162. [PubMed: 6870819]
29. Scollo F, Tempra C, Lolicato F, et al. Phospholipids critical micellar concentrations trigger different mechanisms of intrinsically disordered proteins interaction with model membranes. J Phys Chem Lett. 2018;9:5125–5129. [PubMed: 30133296]
30. Levental I, Levental KR, Heberle FA. Lipid rafts: controversies resolved mysteries remain. Trends Cell Biol. 2020;30:341–353. [PubMed: 32302547]
31. van Meer G, Voelker DR, Feigenson GW. Membrane lipids: where they are and how they behave. Nat Rev Mol Cell Biol. 2008;9:112–124. [PubMed: 18216768]
32. Alecu I, Bennett SAL. Dysregulated lipid metabolism and its role in alpha-synucleinopathy in Parkinson's Disease. Front Neurosci. 2019;13:328. [PubMed: 31031582]
33. Galvagnion C, Buell AK, Meisl G, et al. Lipid vesicles trigger α-synuclein aggregation by stimulating primary nucleation. Nat Chem Biol. 2015;11:229–234. [PubMed: 25643172]
34. Matveyenka M, Rizevsky S, Kurouski D. Unsaturation in the fatty acids of phospholipids drastically alters the structure and toxicity of insulin aggregates grown in their presence. J Phys Chem Lett. 2022;13:4563–4569. [PubMed: 35580189]
35. Matveyenka M, Rizevsky S, Kurouski D. The degree of unsaturation of fatty acids in phosphatidylserine alters the rate of insulin aggregation and the structure and toxicity of amyloid aggregates. FEBS Lett. 2022;596:1424–1433. [PubMed: 35510803]
36. Kurouski D, Luo H, Sereda V, Robb FT, Lednev IK. Rapid degradation kinetics of amyloid fibrils under mild conditions by an archaeal chaperonin. Biochem Biophys Res Commun. 2012;422:97–102. [PubMed: 22564742]
37. De Simone A, Naldi M, Tedesco D, et al. Investigating in vitro amyloid peptide 1-42 aggregation: impact of higher molecular weight stable adducts. ACS Omega. 2019;4:12308–12318. [PubMed: 31460348]
38. Kurouski D, Lombardi RA, Dukor RK, Lednev IK, Nafie LA. Direct observation and pH control of reversed supramolecular chirality in insulin fibrils by vibrational circular dichroism. Chem Commun. 2010;46:7154–7156.
39. Barth A. Infrared spectroscopy of proteins. Biochim Biophys Acta. 2007;1767:1073–1101. [PubMed: 17692815]
40. Sarroukh R, Goormaghtigh E, Ruysschaert JM, Raussens V. ATR-FTIR: a “rejuvenated” tool to investigate amyloid proteins. Biochim Biophys Acta. 2013;1828:2328–2338. [PubMed: 23746423]
41. Rizevsky S, Zhaliazka M, Dou T, Matveyenka M. Characterization of substrates and surface-enhancement in atomic force microscopy infrared (AFM-IR) analysis of amyloid aggregates. J Phys Chem C. 2022;126:4157–4162.
42. Ruggeri FS, Longo G, Faggiano S, Lipiec E, Pastore A, Dietler G. Infrared nanospectroscopy characterization of oligomeric and fibrillar aggregates during amyloid formation. Nat Commun. 2015;6:7831. [PubMed: 26215704]
43. Ruggeri FS, Mannini B, Schmid R, Vendruscolo M, Knowles TPJ. Single molecule secondary structure determination of proteins through infrared absorption nanospectroscopy. Nat Commun. 2020;11:2945. [PubMed: 32522983]
44. Dazzi A, Prater CB. AFM-IR: technology and applications in nanoscale infrared spectroscopy and chemical imaging. Chem Rev. 2017;117:5146–5173. [PubMed: 27958707]
45. Kurouski D, Dazzi A, Zenobi R, Centrone A. Infrared and Raman chemical imaging and spectroscopy at the nanoscale. Chem Soc Rev. 2020;49:3315–3347. [PubMed: 32424384]
46. Dou T, Li Z, Zhang J, Evilevitch A, Kurouski D. Nanoscale structural characterization of individual viral particles using atomic force microscopy infrared spectroscopy (AFM-IR) and tip-enhanced raman spectroscopy (TERS). Anal Chem. 2020;92:11297–11304. [PubMed: 32683857]

47. Ruggeri FS, Flagmeier P, Kumita JR, et al. The influence of pathogenic mutations in alpha-synuclein on biophysical and structural characteristics of amyloid fibrils. ACS Nano. 2020;14:5213–5222. [PubMed: 32159944]

48. Rizevsky S, Matveyenka M, Kurouski D. Nanoscale structural analysis of a lipid-driven aggregation of insulin. J Phys Chem Lett. 2022;13:2467–2473. [PubMed: 35266717]

49. Ramer G, Ruggeri FS, Levin A, Knowles TPJ, Centrone A. Determination of polypeptide conformation with nanoscale resolution in water. ACS Nano. 2018;12:6612–6619. [PubMed: 29932670]

50. Cataldi R, Chia S, Pisani K, et al. A dopamine metabolite stabilizes neurotoxic amyloid-beta oligomers. Commun Biol. 2021;4:19. [PubMed: 33398040]

51. Viennet T, Wordehoff MM, Uluca B, et al. Structural insights from lipid-bilayer nanodiscs link alpha-Synuclein membrane-binding modes to amyloid fibril formation. Commun Biol. 2018;1:44. [PubMed: 30271927]

52. Giasson BI, Murray IV, Trojanowski JQ, Lee VM. A hydrophobic stretch of 12 amino acid residues in the middle of alpha-synuclein is essential for filament assembly. J Biol Chem. 2001;276:2380–2386. [PubMed: 11060312]

53. Ueda K, Fukushima H, Masliah E, et al. Molecular cloning of cDNA encoding an unrecognized component of amyloid in Alzheimer disease. Proc Natl Acad Sci U S A. 1993;90:11282–11286. [PubMed: 8248242]

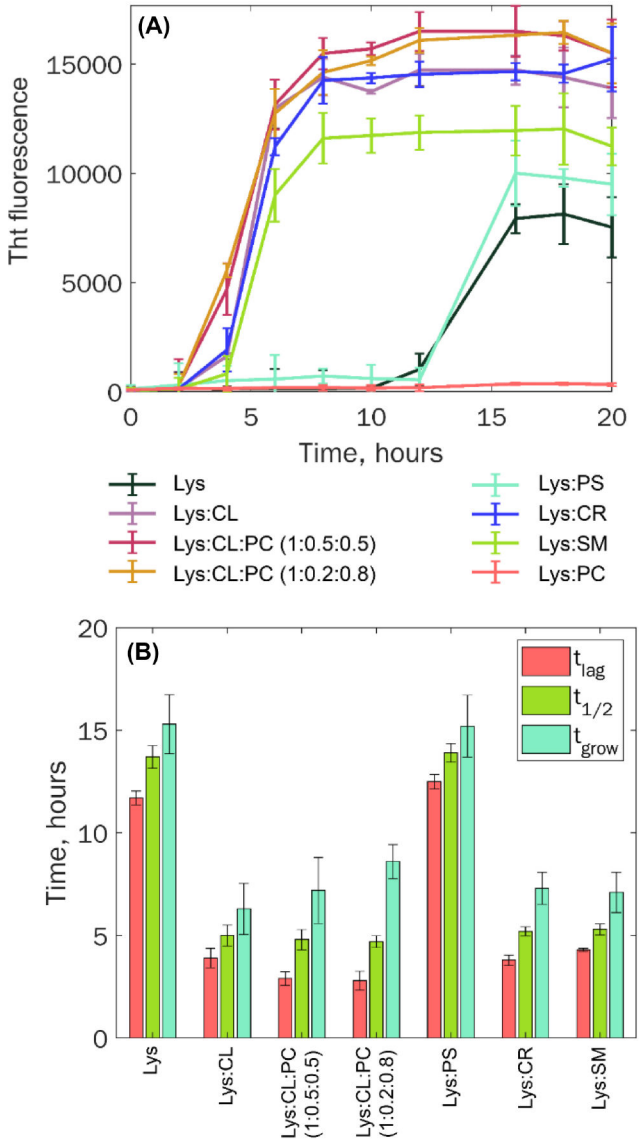

FIGURE 1.

Lipids uniquely alter the rate of lysozyme aggregation. ThT aggregation kinetics (A) of lysozyme in the lipid-free environment (Lys) and in the presence of CL, CER, PS, PC, and SM at 1:1 molar ratios, as well as in the presence of lipid mixtures PC:CL at 1:1 and 0.8:0.2. Corresponding tlag, t1/2 and tgrow values (B) indicate aggregation time when the intensity of ThT fluorescence reached 10% (tlag), 50% (t1/2) and 90% (tgrow). For Lys, 400 μM of protein was dissolved in 1× PBS with 2 mM of ThT; pH adjusted to pH 3.0. For Lys:CL, Lys:CER, Lys:PS, and Lys:SM, as well as for Lys:PC:CL (1:0.5:0.5) and Lys:PC:CL (1:0.8:0.2), 400 μM of lysozyme was mixed with an equivalent concentration of the corresponding lipid; pH was adjusted to pH 3.0. All samples were kept in a dry block-heater and kept at 65°C for 24 h. ThT measurements were made every 2 h.

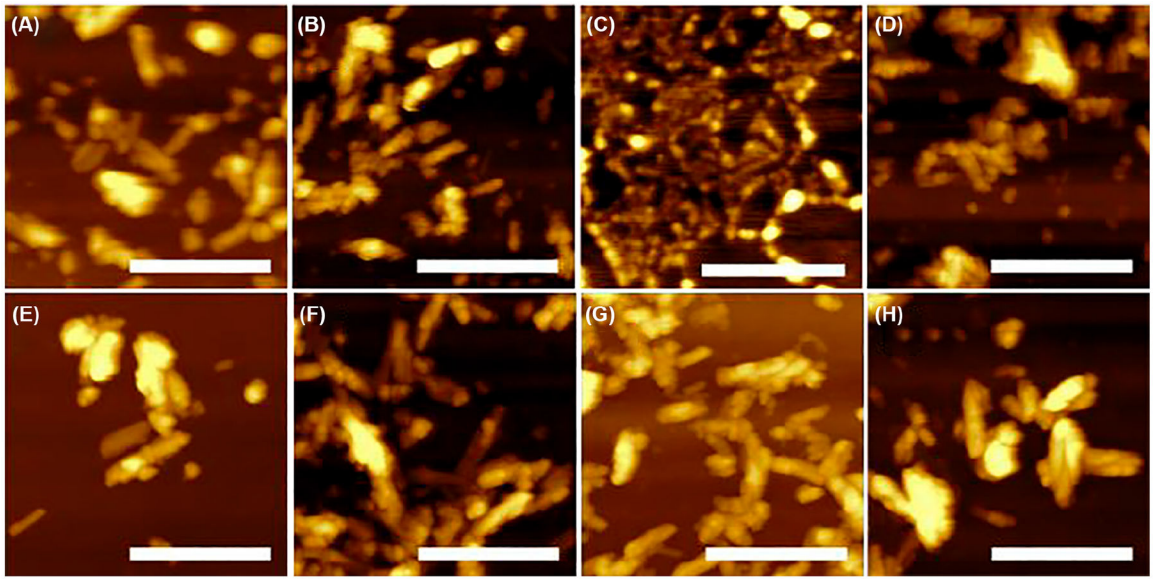

FIGURE 2.

Lipids uniquely alter morphologies of lysozyme aggregates. AFM images of Lys aggregates (A), Lys:PS (B), Lys:PC (C), Lys:CL (D), Lys:PC:CL (1:0.5:0.5) (E), Lys:PC:CL (1:0.8:0.2) (F), Lys:SM (G), and Lys:CER (H). After 24 h of incubation of lysozyme (400 μM) with and without lipids at 65°C, sample aliquots were diluted with 1× PBS pH 3.0 and deposited onto the pre-cleaned silicon wafer. AFM imaging was performed in tapping mode. Scale bars are 500 nm.

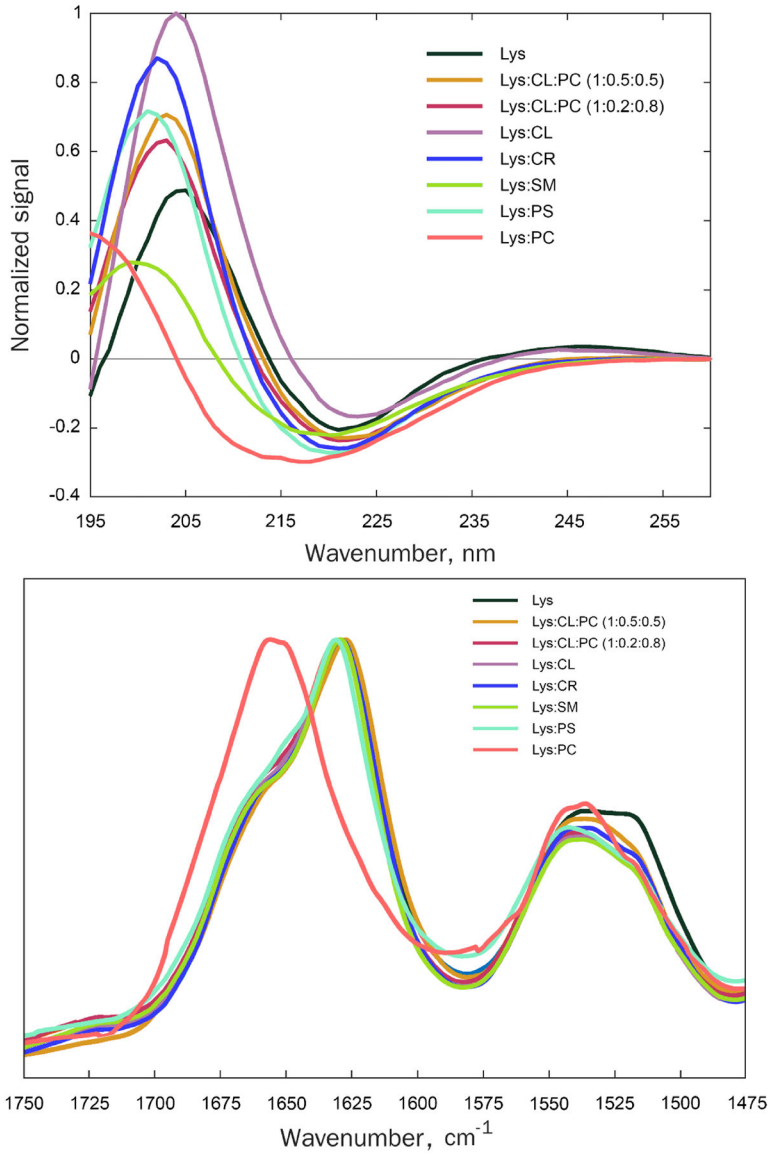

FIGURE 3.

Structural analysis of lysozyme aggregates. CD (top) and ATR-FTIR (bottom) spectra of lysozyme aggregates (Lys) grown in the lipid-free environment (black), Lys:CER (green), Lys:CL (blue), Lys:PC (gray), Lys:SM (yellow), Lys:PS (brown), Lys:PC:CL (1:0.5:0.5, navy) and Lys:PC:CL (1:0.8:0.2, purple). After 24 h of incubation of lysozyme (400 μM) with and without lipids at 65°C, triplicates of samples were diluted with 1× PBS pH 3.0 and placed into quartz cuvette (CD) or directly deposited onto ATR crystal (ATR-FTIR) and dried under room temperature. For each of the presented traces, three independent CD or ATR-FTIR measurements were averaged.

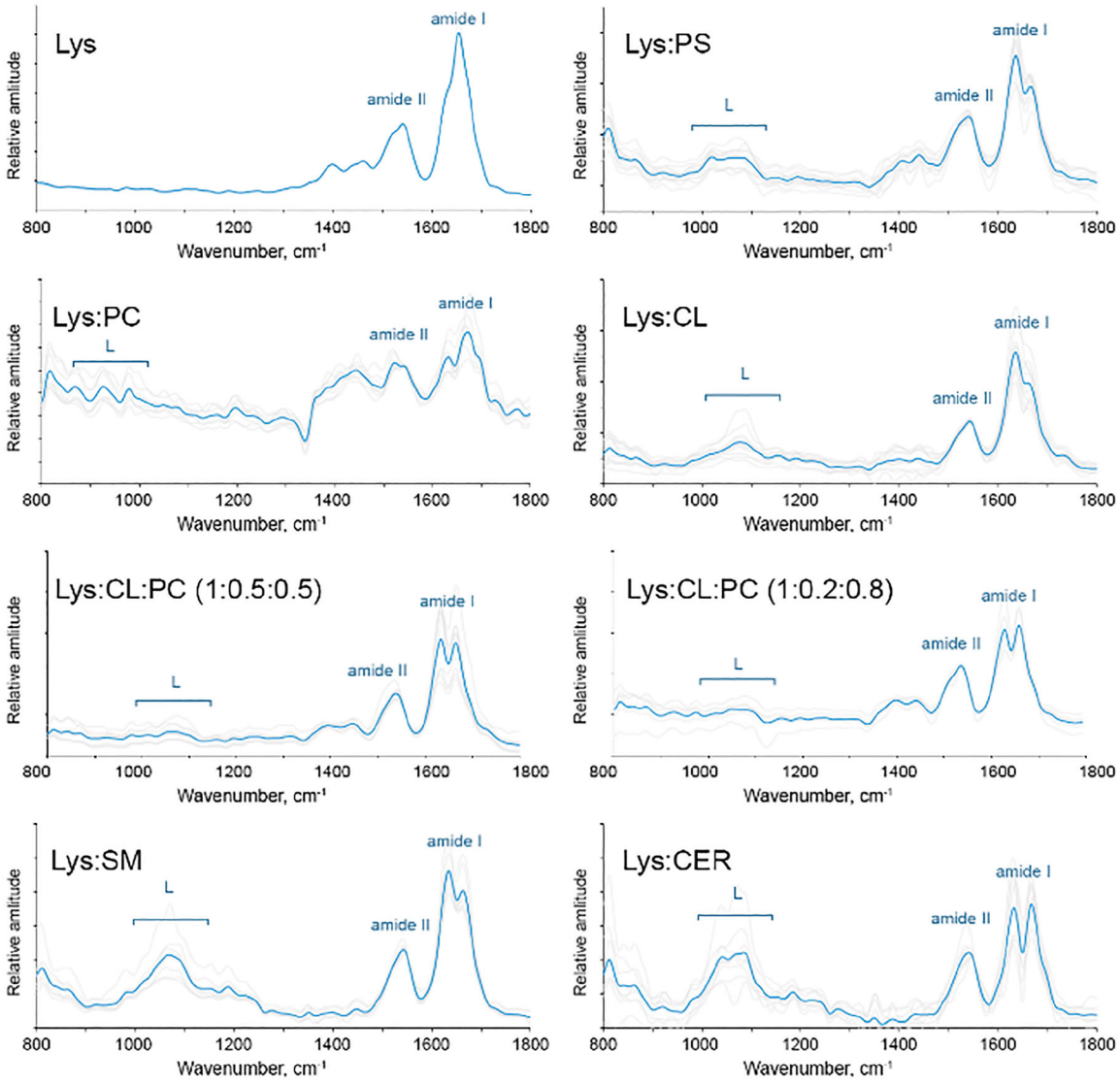

FIGURE 4.

Nanoscale analysis of lipid content of lysozyme aggregates. AFM-IR spectra of lysozyme aggregates grown in the absence of lipids (Lys) and the presence of PS, PC, CL, as Lys:PC:CL (1:0.5:0.5), as Lys:PC:CL (1:0.8:0.2), SM, and CER. Spectra collected from individual aggregates are in gray, whereas the corresponding average spectra are in blue. After 24 h of incubation of lysozyme (400 μM) with and without lipids at 65°C, sample aliquots were diluted with 1× PBS pH 3.0 and deposited onto the pre-cleaned silicon wafer. AFM-IR analysis was performed in contact mode. At least 30–40 individual aggregates were analyzed for each sample.

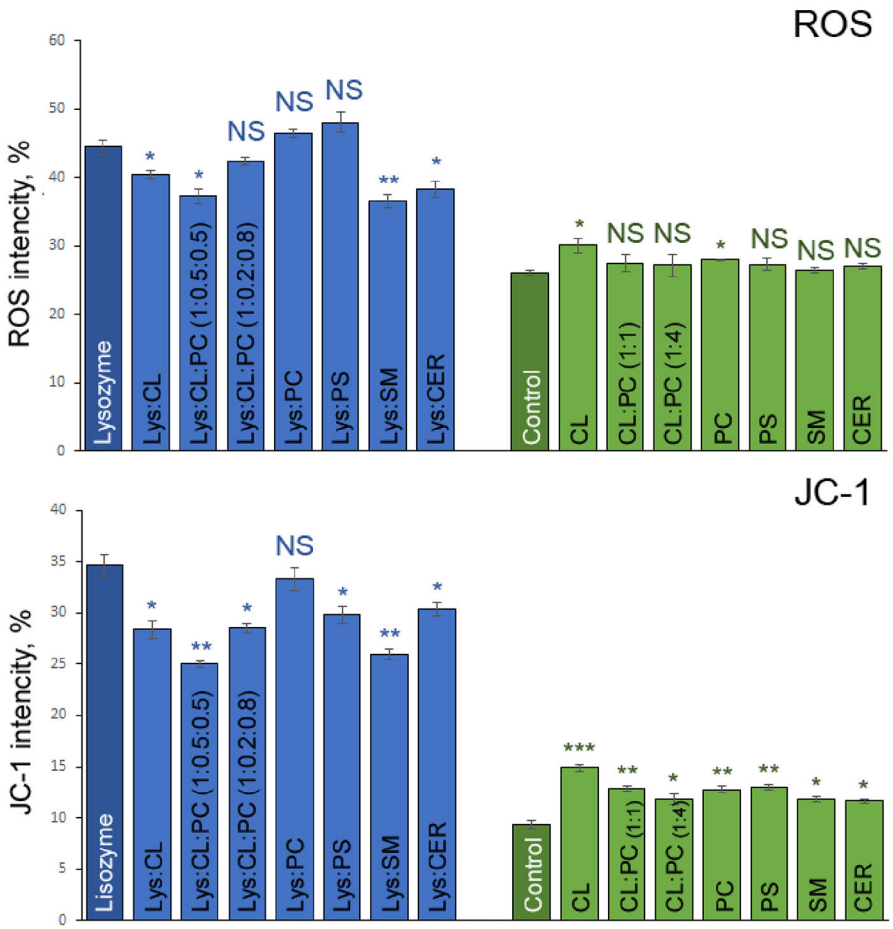

FIGURE 5.

Lysozyme aggregates grown in the presence of lipids possess lower cell toxicity compared to the aggregates grown in a lipid-free environment. Histograms of ROS (top) and JC-1 (bottom) toxicity assays of Lys, Lys:CL, Lys:CL:PC (1:0.5:0.5), Lys:CL:PC (1:0.2:0.8), Lys:PC, Lys:PS, Lys:SM, and Lys:CER, as we as lipids themselves (CL, CL:PC (1:1), CL:PC (1:4), PC, PS, SM, and CER). After 24 h of incubation of lysozyme (400 μM) with and without lipids at 65°C, sample triplicates were exposed to mice midbrain N27 cells for 48 h. For each of the presented results, three independent measurements were made.

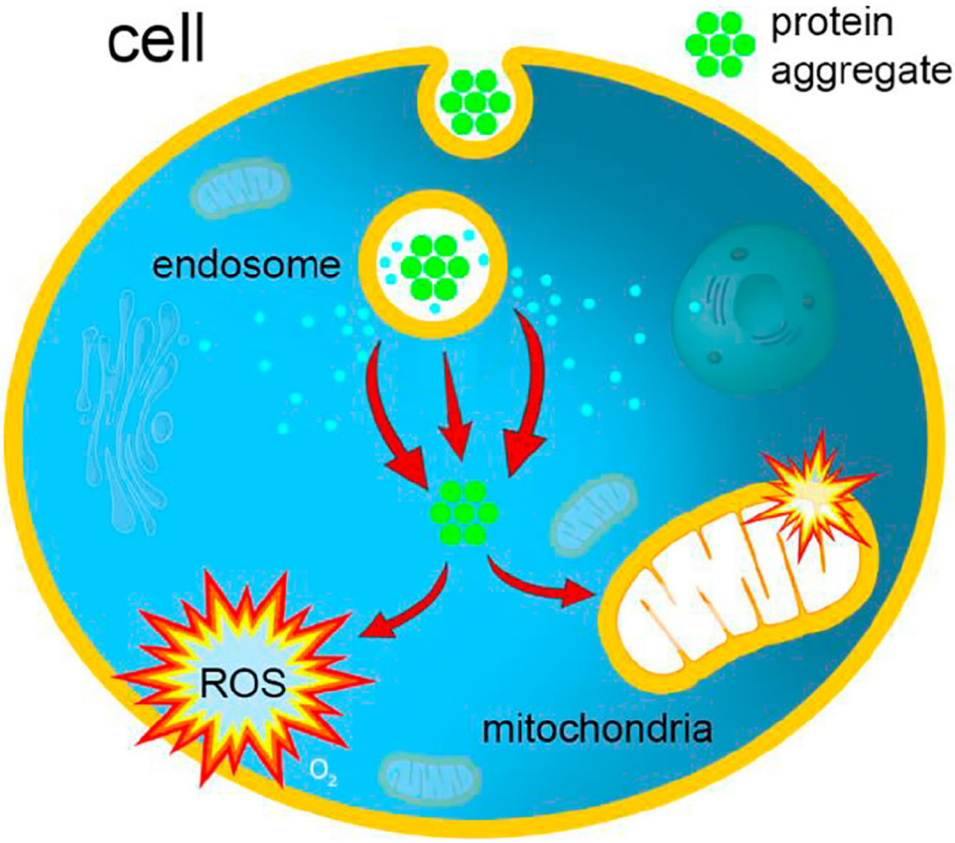

FIGURE 6.
Mechanism of cell toxicity exerted by lysozyme aggregates.